

ONE- VS TWO- OR THREE-DIMENSIONAL EFFECTS IN SEDIMENTARY VALLEYS

Jacobo BIELAK¹, Yoshiaki HISADA², Hesheng BAO³, Jifeng XU⁴ And Omar GHATTAS⁵

SUMMARY

This study of the effects of local geological conditions on seismic ground motion uses 1D amplification as a reference point and examines, via simple theoretical and more realistic numerical examples and observations, how 2D and 3D conditions differ from 1D estimations. Because 1D simulations cannot model basin and edge effects, 1D response tends, in general, to exhibit lower peaks and be of shorter duration than 2D and 3D results. On the other hand, due to destructive interference of different types of waves, there are sites where the response can be much smaller than predicted by 1D models.

INTRODUCTION

It has long been known that local geological conditions can strongly influence ground motion during earthquakes (Matsuzawa, 1926). The importance of these effects became dramatically apparent during the 1985 Michoacán earthquake, which caused widespread damage in Mexico City, at a distance of 400 km from the epicenter. Damage was extensive to structures located within the lakebed region, but was minimal or nonexistent outside the soft soil deposits. Since then, the 1988 Spitak, 1989 Loma Prieta, 1994 Northridge, and 1995 Hyogoken-Nambu (Kobe) earthquakes have underscored the importance of the effects of site conditions on ground response. In particular, the toll from the Kobe earthquake was huge, in excess of 5000 dead and 200US billion dollars in direct material losses even though its magnitude (6.8) was of the same order as that of the Northridge earthquake, which caused severe, but far less damage. Most of the damage in the city of Kobe occurred within the so-called “disaster belt,” a narrow strip 1 km wide and 20 km long about 1 km away from the Osaka basin. The combined effects of the source (the forward directivity effects, e.g., Wald (1995)) and the site (the basin edge effects, e.g., Kawase (1966)) probably caused the large ground motion within the belt.

Local site effects are generally taken into consideration in seismic provisions of building codes by means of a specified amplification factor applied to the spectral acceleration coefficient. This amplification factor depends either on the type of surficial soil at the site (e.g., NEHRP, 1997) or on the location of the site (e.g., Mexico City Building Code, Reglamento, 1993). In both cases, the value of this amplification factor is derived from observations and from one-dimensional (1D) amplification studies. Evidence from recent earthquakes, however, indicates that 2D and 3D site effects on ground motion are often important. It remains controversial whether in practice it is sufficient to consider 1D models or whether 2D or 3D models are necessary to evaluate realistically the site effects, since 1D models neglect completely the surface waves.

In this paper we summarize key results of 1D dynamic amplification of soil deposits and review, using observations and results from simulations, key aspects of the 2D and 3D site effects on soil response in sedimentary valleys. We restrict our discussion to the linear range of response.

¹ Department of Civil and Environmental Engineering, Carnegie Mellon University, Pittsburgh PA, USA; jbielak@cmu.edu

² Kogakuin University, Department of Architecture, Tokyo, Japan

³ Algor, Inc., Pittsburgh, PA, USA

⁴ Lam Research, Inc., Fremont, CA, USA

⁵ Department of Civil and Environmental Engineering, Carnegie Mellon University, Pittsburgh, PA, USA

ONE-DIMENSIONAL EFFECTS

One argument advanced by engineers to justify the use of vertically incident waves as the excitation is that the incoming body waves tend to become vertical as they travel upwards, as a consequence of Snell's law. This is illustrated in Fig. 1, which shows the particle displacements on a vertical cross-section of the San Fernando

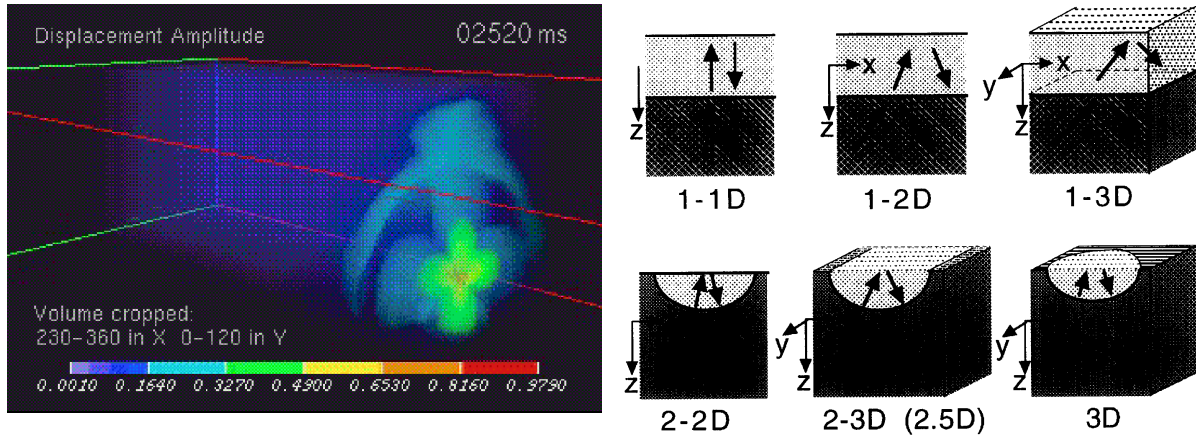


Figure 1. (a) Instantaneous displacement pattern in San Fernando Valley (from Quake animation, www.cs.cmu.edu/~quake; (b) Dimensionality of problems used for studies of site effects (Hisada and Yamamoto, 1996)

Valley due to a double couple applied at a point 11 km deep at a dip angle of 44° , representing an aftershock of the 1994 Northridge earthquake. Naturally, the excitation for an extended fault is far more complex.

To fix ideas concerning 1D amplification in layered systems it is useful to consider the simple case of a single elastic layer of thickness H underlain by an elastic halfspace, as shown on the top left corner diagram of Fig. 1b. This case has been studied by many investigators (e.g., Kanai et al (1959), Herrera and Rosenblueth (1965), Roesset, (1970)). We consider a vertically incident steady-state harmonic SH-wave of unit amplitude and frequency ω . The amplitude of the displacement, u , at the free-field surface at the top of the layer is then given by:

$$|u|/|w| = \left[\cos^2(\omega H/V_s) + \alpha^2 \sin^2(\omega H/V_s) \right]^{-1/2} \quad (1)$$

In this equation, w is the amplitude of the displacement that would occur at the top of the halfspace if the layer were not present. Hence, the ratio $|u|/|w|$ then represents the amplification of a layer of density ρ_s , and shear wave velocity V_s with respect to that of the halfspace alone. ρ_r and V_r are the corresponding values for the halfspace, and $\alpha = \rho_s V_s / \rho_r V_r$ is the impedance ratio. From (1) it follows that $|u|/|w|$ attains maximum and minimum values at frequencies $\omega_m H/V_s = (2m-1)\pi/2, m\pi/2, m=1,2,\dots$, respectively. Notice that the resonant frequencies depend only on the layer thickness and shear wave velocity, independently of the properties of the halfspace. The same is true for the frequencies for which the response is minimum. The corresponding values of the amplification ratios are $1/\alpha$ and unity. These values decrease if damping is incorporated into the soil model (see, e.g., Roesset, 1970). For multiple layers the response is qualitatively similar, except that the separation between resonant frequencies becomes variable and the corresponding peaks take different values.

TWO-DIMENSIONAL EFFECTS

To examine the effect that lateral confinement has on the resonant frequencies of a layer, we consider initially the extreme case of a box of rectangular cross section of width L , height H , and infinite length. The box, which is fixed at the bottom and lateral sides, and free at the top, is filled with a homogeneous material of density ρ_s and shear wave velocity V_s . Bard and Bouchon (1985) and Bielak et al (1999) considered this example to help explain the behavior of 2D valleys under SH excitation. The natural frequencies of this valley, normalized with respect to the fundamental frequency of the single layer, are given by:

$$\omega_{mn}/\omega_1 = \left[(2m-1)^2 + n^2(2H/L)^2 \right]^{1/2}; m, n = 1, 2, \dots \quad (2)$$

This expression shows that the valley has a double set of natural frequencies. The first term on the rhs corresponds precisely to the m th resonant frequency of the infinite layer without lateral confinement. The second term reflects the influence of the lateral walls. For each natural frequency of the flat layer there is an infinite set

of frequencies stemming from the lateral confinement. Associated with each frequency ω_{mn} there is a natural mode, u_{mn} , given by:

$$u_{mn} = \sin\left[\frac{(2m-1)\pi y}{2L}\right] \sin\left(\frac{n\pi x}{L}\right), m, n = 1, 2, \dots \quad (3)$$

The origin of the coordinate system is at the lower left corner of the valley, the horizontal x-axis along the width, and the vertical y-axis toward the free surface. The first factor on the rhs gives the modal shapes of the flat layer while the second is the modification due to the finite lateral length of the valley. The modes have nodes along the free surface, where the displacement vanishes. One way to interpret these nodes is to regard the motion in the valley as consisting of waves. There are body waves traveling upwards from the bottom of the valley that get reflected at the free surface. In addition, surface waves, which are generated at the two lateral edges of the valley travel from one edge to the other. For large or open basins these surface waves dissipate due to attenuation before they reach the opposite edge. In either case, large response occurs when upward and lateral waves at a point have the same sign. Cancellation occurs at the nodes when the two waves have opposite signs. These are forms of constructive and destructive interference that can be observed in more complex situations. For instance, Bielak et al (1999) simulated the ground motion in a small, closed, valley in Kirovakan, located near the epicenter of the 1985 Spitak earthquake in Armenia to try to explain observed damage for which 1D analyses had substantially underpredicted the ground surface motion (Yegian et al, 1994). Figure 2a shows the 1D and 2D amplification ratios (AR) at a point in the middle of the valley as a function of the frequency of excitation, with

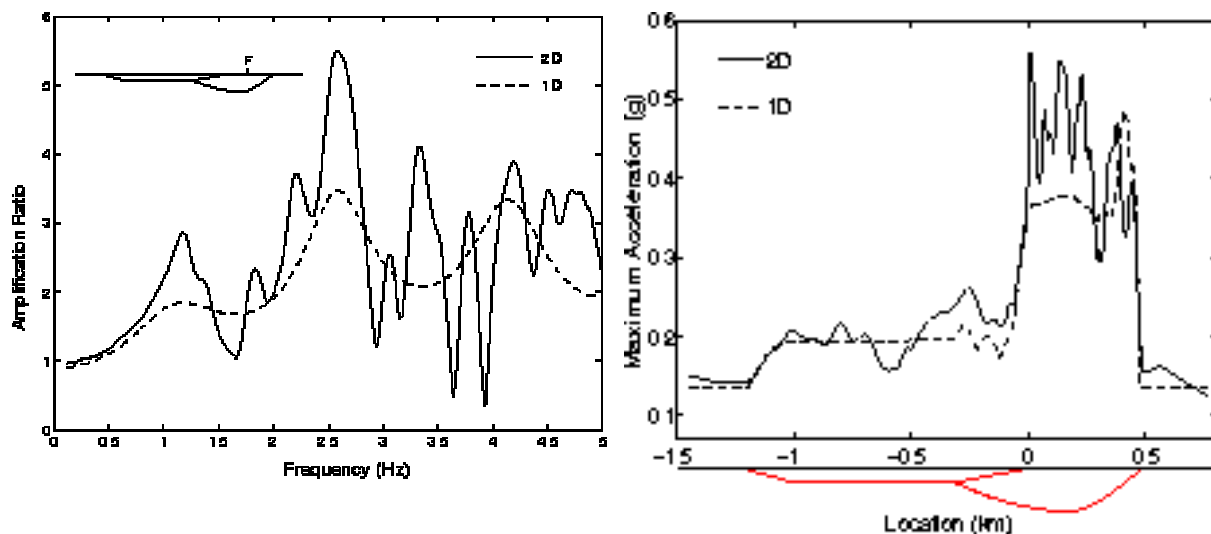


Figure 2. (a) 1D and 2D amplification ratios at site F (see insert) due to steady-state harmonic vertically incident SH-wave; (b) Maximum free surface 1D and 2D synthetic accelerations across a valley in Kirovakan during Spitak earthquake. Bielak et al (1999).

respect to the free-field response. For the frequency range considered, the AR exhibits three resonance frequencies, at somewhat shorter intervals than for a single layer, and the peak values no longer have a constant value as for the single layer. The 2D amplification ratio also exhibits resonant behavior in the vicinity of the 1D resonant frequencies, but the corresponding 2D frequencies are slightly higher than those for the 1D results, due to the lateral confinement of the valley. The values of the respective peaks, however, are considerably larger for the 2D case. In addition to the essentially 1D resonant frequencies, the 2D valley exhibits resonant behavior at other frequencies, similarly to the simple box. The amplification ratio oscillates rapidly with frequency, reaching peak values that greatly exceed the 1D values. Interestingly, for certain frequencies the 2D amplification ratio is much smaller than unity, denoting in effect a strong deamplification of seismic waves akin to that observed for the box. In addition to steady-state excitation, the 1D transient response of the valley was calculated for a transient incoming wave based on a reference acceleration recorded during the 1994 Spitak earthquake. Figure 2b shows the spatial variation of the peak ground acceleration along the entire valley, corresponding to both 2D and 1D simulations. The peak response is highly oscillatory within the softer portion of the valley, exhibiting marked edge effects at the two margins of the valley. At the right edge both 1D and 2D peak accelerations are large, as a consequence of the large impedance contrast between the softest soil near the free surface and the surrounding rock. At the left margin, the 2D response is markedly higher than for 1D, the difference being due to wave diffraction and surface waves.

A similar but more pronounced edge effect was obtained by Adams et al (1999) in a simulation of the response in the Lower-Hutt Valley in New Zealand, due to a Ricker pulse with a central frequency that coincides with the fundamental 1D resonant frequency of the deeper part of the valley. The 1D and 2D transient response is depicted in Fig. 3 as a set of surface ground velocity seismograms along the entire length of the valley. Notice

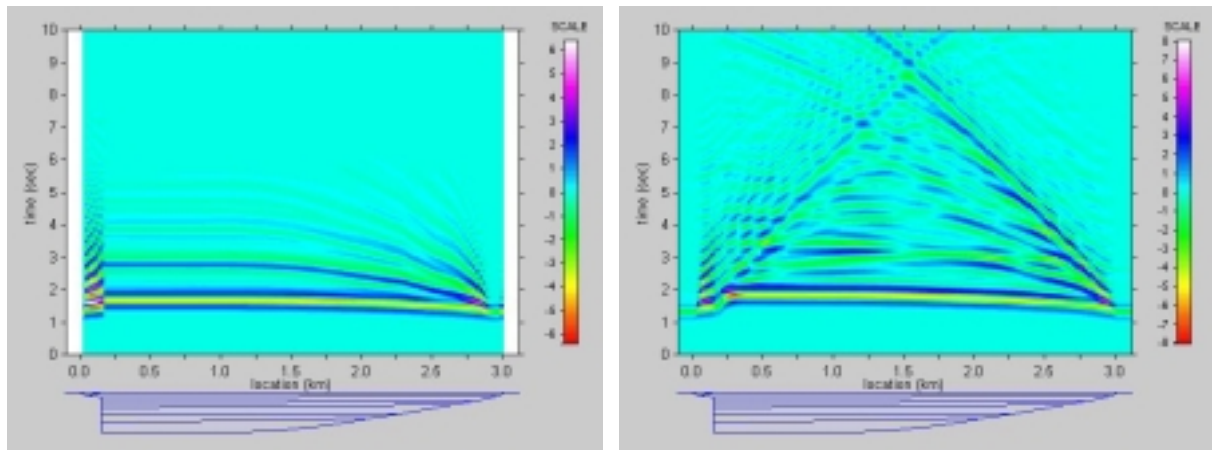


Figure 3. (a) 1D and (b) 2D synthetic velocity across a model of Lower Hut, NZ; vertically incident SH-wave with a Ricker pulse excitation with central frequency of 2 Hz (Adams et al, 1999; Adams, personal comm. 1999).

the clear trace of the surface wave in the 2D simulation and the large 2D amplification near the left edge caused by the steep discontinuity between the valley and the surrounding rock. Although this valley is closed, surface waves do not reach the opposite edges during the strong motion phase due to the large extent of the valley.

Figure 4 provides another illustration of 2D site effects on ground motion, for an open basin. It shows the 2D

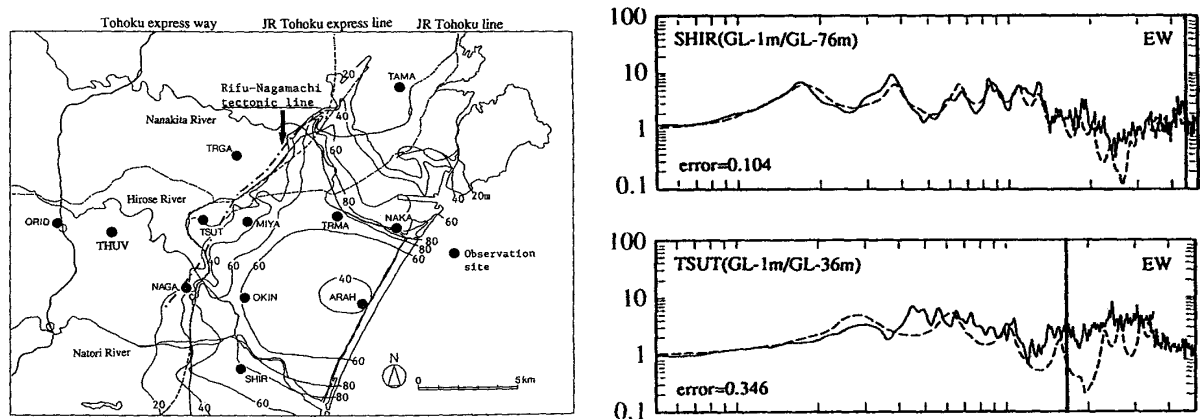


Figure 4. (a) Map of Yokohama indicating location of instrumented sites; (b) observed and synthetic spectral 1D ratios at STUT and SHIR stations due to an actual earthquake (Sato et al, 1996)

spectral, or amplification, ratios at two locations in the Sendai vicinity in Japan obtained by Satoh et al (1995) from records registered during an actual earthquake. The location SHIR and TSUT are identified in Fig. 4a. Also shown are results of 1D simulations by these authors using soil properties determined through an inversion process. The similarity between the 1D simulation results and the direct observations at SHIR is quite striking. This indicates that a 1D analysis is sufficient for determining site effects at SHIR, which is located in the central portion of the basin. By contrast, at STUT, which is located closer to the basin edge, 2D effects similar to those calculated for Kirovakan are observed.

THREE-DIMENSIONAL EFFECTS

The occurrence of recent earthquakes in highly populated regions has spurred the placement of instruments for recording strong ground motion in basins. In addition, the advent of powerful workstations and parallel computers and the desire to gain a better understanding of the spatial and temporal distribution of ground motion in basins has enabled investigators to conduct 3D simulations of ground motion using realistic models (e.g., Frankel, 1993; Graves, 1996; Olsen and Archuleta, 1996; Bao et al, 1998; Pitarka and Irikura, 1998). In this section we present several simulation results and observations to highlight some of the 3D effects of surface geology on ground response to earthquakes.

We start with a simple model shown in Fig. 5a of an idealized closed basin, first used by Sánchez-Sesma and Luzón (1995). The basin consists of soil whose shear wave velocity is one half that of the exterior medium and is

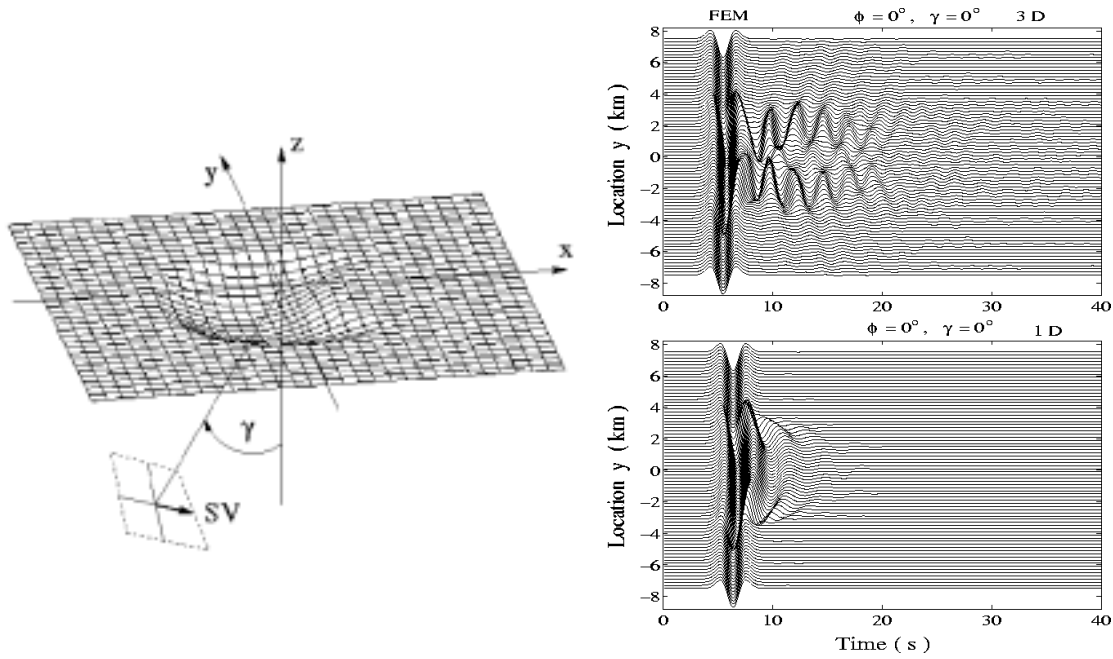


Figure 5. (a) Plan view of idealized (Moon) basin; (b) 1D and 3D synthetic horiz. displacements (Bao, 1998).

subjected to a Ricker pulse travelling in the form of an incident SV-wave with a central frequency equal to the 1D fundamental frequency of the basin at the deepest point (Bao, 1998). Figure 5b shows synthetics of the horizontal velocity along the y-axis for a vertically incident wave with particle motion polarized along the x-axis. Also shown is the corresponding 1D simulation. There are two main differences between the two sets of results. First, the larger peak of the 3D response and second, its significantly extended duration. Figure 6a shows the

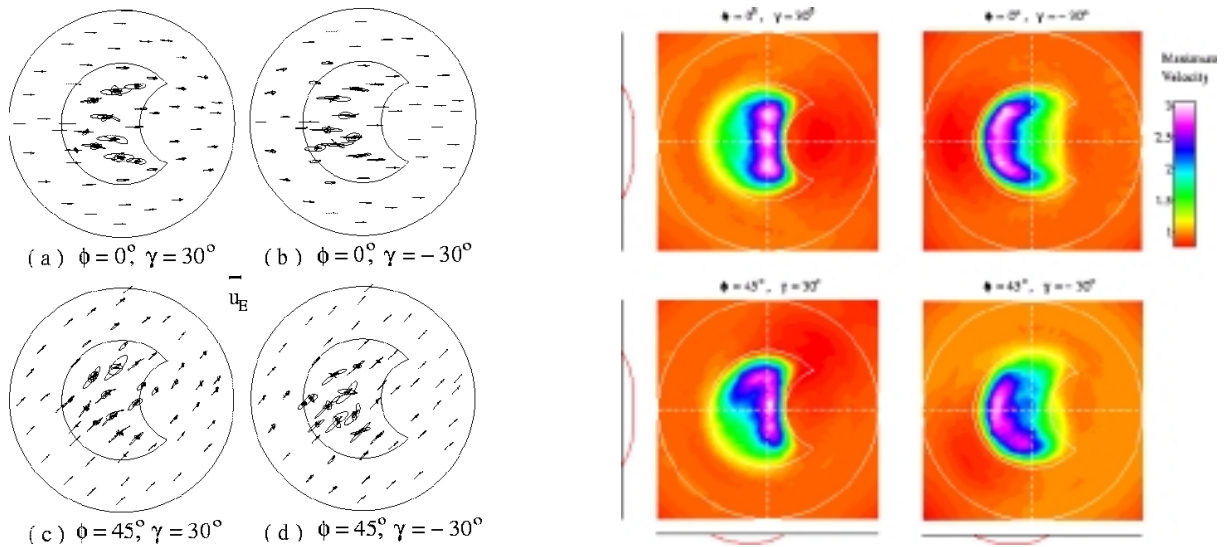


Figure 6. (a) Synthetic seismoscope trace of horizontal displacement at several locations within the Moon basin and its vicinity due to Ricker pulse excitation; (b) Distribution of maximum horiz. velocities (Bao, 1998).

particle orbits on the horizontal plane at a number of points throughout the basin for different azimuths of the incoming wave. This angle, denoted as ϕ is measured from the x-axis. The incident wave makes an angle of 30° with the vertical. While the particle motion generally tends to follow the direction of motion of the incident wave, there is a strong 3D effect characterized by the deviation from the direction of incidence. The distribution of the maximum amplitude of the horizontal velocity with respect to that in the free field is shown in Fig. 6b. The maximum amplification is of the order of 3 for all incident angles. The spatial distribution of the response, however, varies significantly with the angle of incidence. In particular, the surface waves are greatly amplified at the opposite end from which the waves arrive.

Figure 7 shows displacements observed and simulated at two sites in Kobe during an aftershock of the 1995

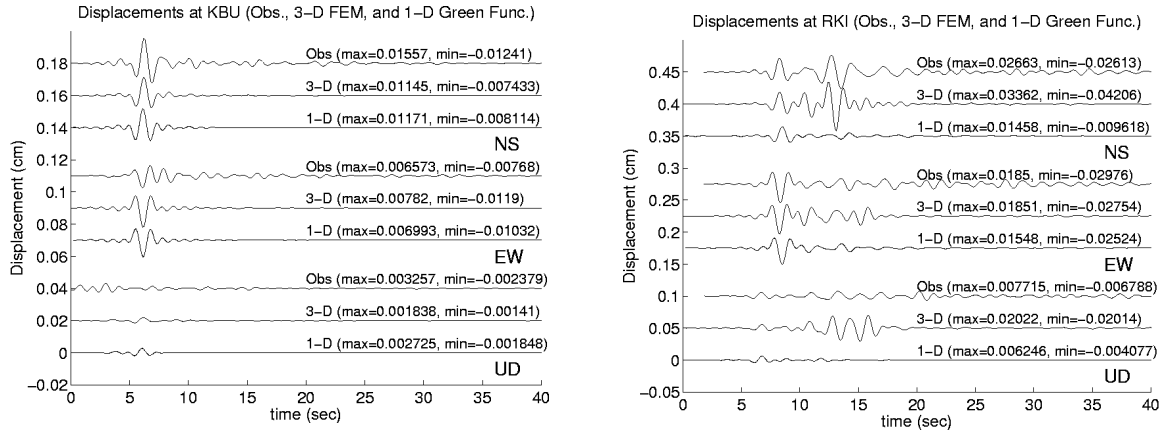


Figure 7. (a) Band-passed displacements (0.9-5.0 s) observed and simulated for a 1995 Kobe earthq. aftershock at sites KBU and RKI (see Fig. 10a) (Hisada et al, 1998).

Kobe earthquake. The location of these sites can be seen in Fig. 10a. Due to the large extent of Osaka Bay the ground motion in Kobe City essentially corresponds to that in an open basin. All the records are band-passed filtered for 0.9-5 seconds (Hisada et al, 1998). For the simulations denoted as GRN we used the Green-function method of Hisada (1995), assuming a 3D wavefield in the 1D flat-layered structure below each site. The simulations labeled FEM are fully 3D. They use a 3D model of the Kobe region and the FEM to calculate the ground motion (Bao et al, 1998). Records denoted as OBS are observations. For KBU, which is located just outside the basin, the GRN and FEM show an excellent agreement with each other and with the actual records. At RKI, a site well inside the basin, the agreement between the 3D simulations and the observations is also excellent. By contrast, the flat-layer simulations exhibit large discrepancies with the observations. The reason for this is that the flat-layered system cannot model the surface waves generated at the edge of the basin, and thus completely misses the strong phase that arrives at about 12 s, which is stronger than the direct wave.

To illustrate how ground motion can vary rapidly over very short distances during actual earthquakes, Fig. 8

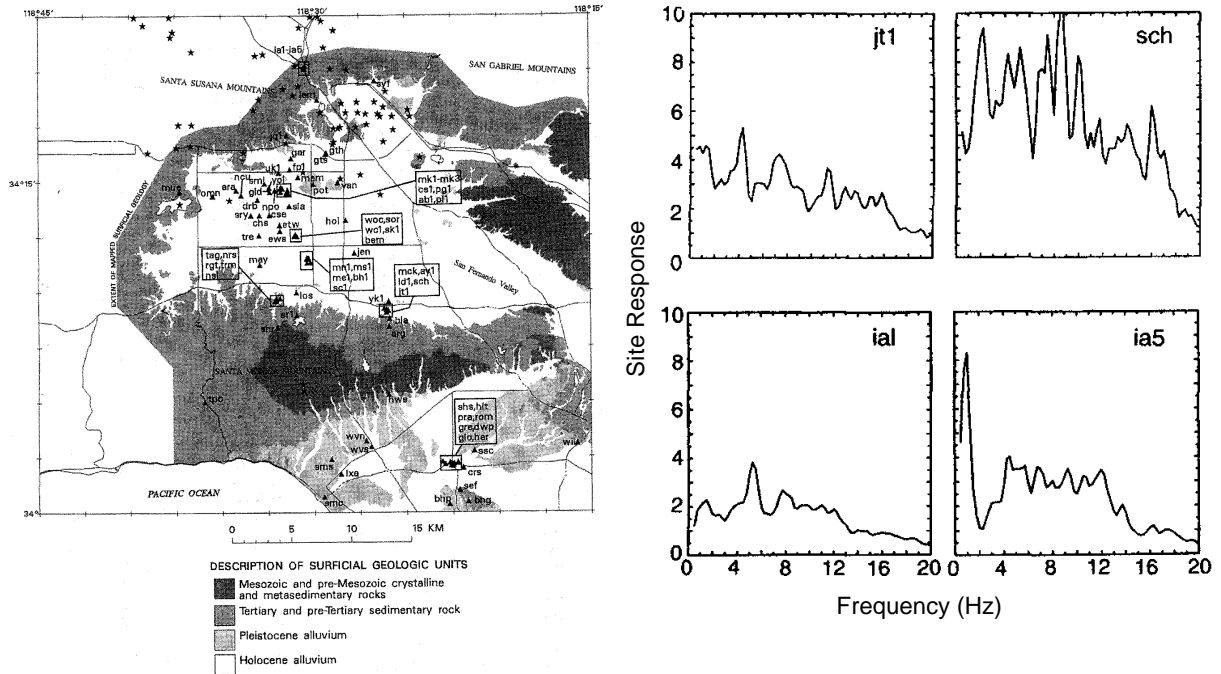


Figure 8. (a) Location of sites in SFV instrumented for studying spatial variation of ground motion of 1994 Northridge earthq. aftershock; (b) spectral ratios at indicated locations derived from recorded seismograms (Hartzell et al, 1996).

shows seismograms of ground motion recorded by Hartzell et al (1996) in two different areas of the San Fernando Valley during aftershocks of the Northridge earthquake. Hartzell et al obtained records at a large number of sites, as shown in Fig. 8a. The Sherman Oaks area, which suffered extensive damage during the main shock is located in the southern part of the valley. Figure 8 shows the spectral ratios at two of these locations, which are separated by less than 100 m. This ratios differ by factors of the order of 3, even at a frequency as low

as 1 Hz. Similar results are observed for the sites ia1 and ia5, located at Interstate 5, just at the northern edge of the valley, nominally on rock.

Graves (1999) performed simulations of the main shock of the 1995 Kobe earthquake over an extended region that covers both Kobe and Osaka, as shown on Fig. 9a. Figure 9b shows comparisons between 3D and flat

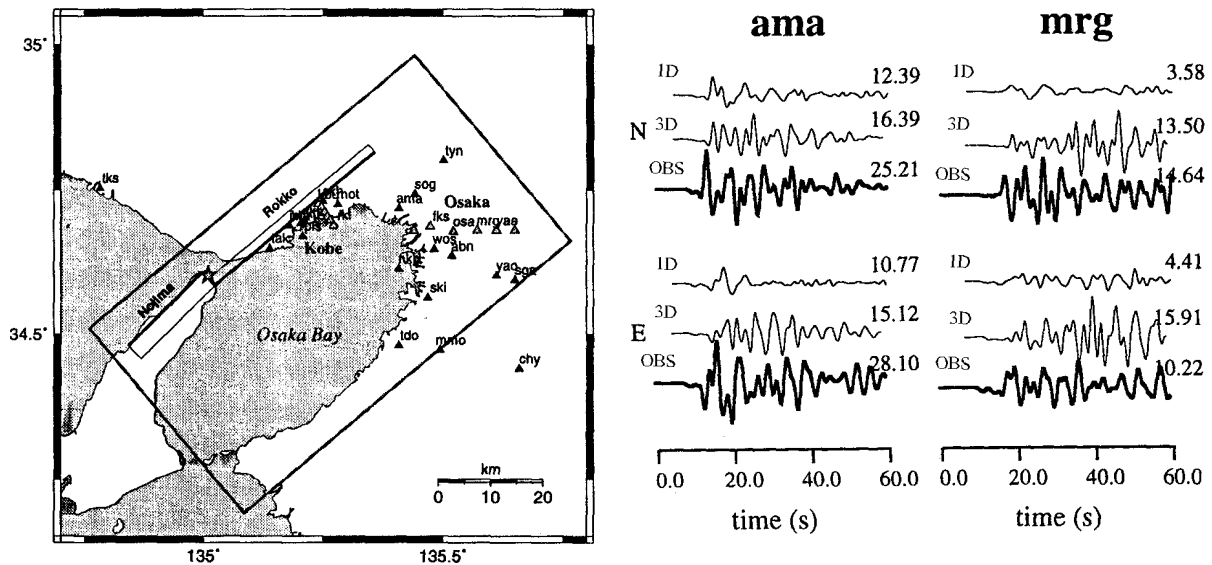


Figure 9. (a) Kobe-Osaka region showing instrumented locations; (b) observed and simulated velocities at two sites during 1995 Kobe earthquake (Graves, 1998).

layered simulations and observations at two sites. The 3D simulations capture the main features of the actual ground motion, albeit with significant quantitative differences. The flat-layered simulations, on the other hand, exhibit much larger differences and completely miss the strong surface waves generated at the northwestern edge of the basin parallel to the causative fault.

Matsushima and Kawase (1999) conducted simulations of Kobe earthquake as well, using a refined model of the geological structure over a limited region comprising the Kobe City surroundings and a detailed model of the source that contains four asperities. Results for the sites FKA, KBU, and RKI (which can be seen in Fig. 10a) are shown in Fig. 10. The agreement between the simulations and the observations is quite close at all three sites.

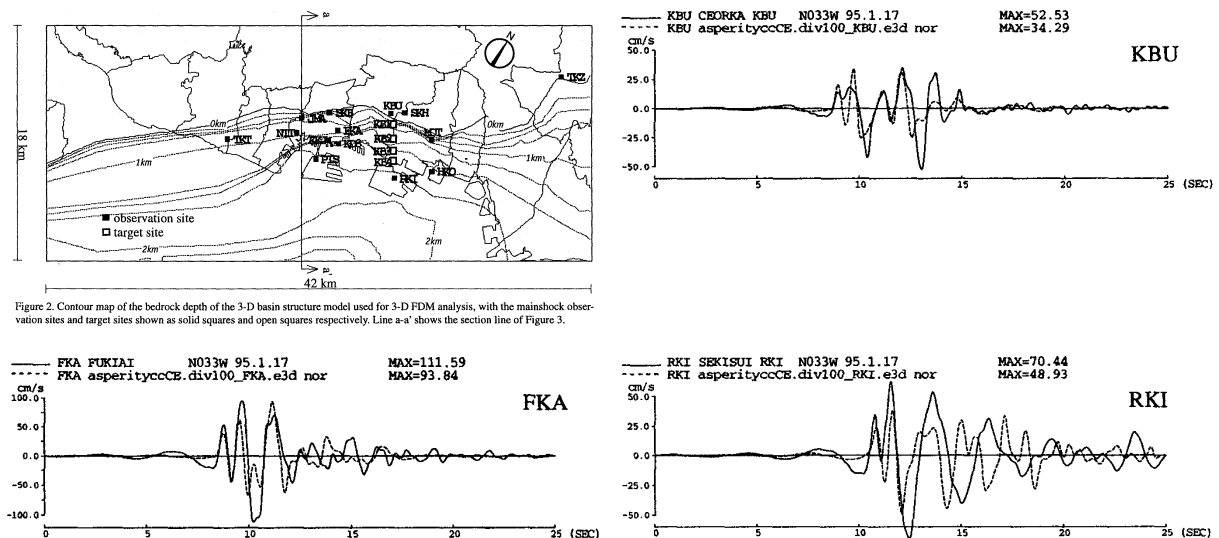


Figure 10. (a) Kobe region showing instrumented locations; (b) observed and simulated velocities at three sites during 1995 Kobe earthquake (Matsushima and Kawase, 1998).

Figure 10. (a) Kobe region showing instrumented locations; (b) observed and simulated velocities at three sites during 1995 Kobe earthquake (Matsushima and Kawase, 1998).

This suggests that model-based simulation show promise as a practical tool for performing the first, critical step in the earthquake resistant design process, which is to assess the ground motion to which a structure will be exposed during its lifetime.

CONCLUDING REMARKS

In this study of the effects of local geological conditions on seismic ground motion, we have used 1D amplification as a reference point and examined, via simple theoretical and more realistic numerical examples and observations, how 2D and 3D conditions differ from 1D estimations. Because 1D simulations cannot model basin and edge effects, 1D response tends, in general, to exhibit lower peaks and be of shorter duration than the corresponding 2D or 3D response. On the other hand, due to destructive interference of different types of waves, there are sites where the response can be much smaller than predicted by 1D models. In fact, one of the most important differences between 1D modeling and 2D, 3D modeling and observations is that while actual ground motion can vary rapidly over short distances even with little or no change in local soil properties, rapid changes in 1D modeling can occur only if the soil properties vary abruptly in the lateral directions. While not yet straightforward, it appears possible to develop seismic design provisions that build on existing ones based on 1D amplification studies for taking local site conditions into consideration. This could be done, for instance, by introducing factors that would incorporate the basin and edge effects as functions of the soil properties underneath the site and of its location with respect to the basin edge. Results of 1D, 2D, and 3D simulations and observations suggest that these factors, however, may vary with frequency.

One final note is in order. Most of the 2D and 3D simulations to date are based on linear soil material models. Energy dissipated due to inelastic behavior, however, causes a reduction in the amplitude of the surface waves that varies exponentially with distance from the edge. Thus, it can be expected that for strong earthquakes edge effects on ground motion are not as large as predicted by purely linear models, especially away from the valley edges. Basin effects from overall local geological structure, on the other hand, can be expected to remain present throughout the basin.

ACKNOWLEDGMENT

We would like to thank Prof. Keiiti Aki for his continuous encouragement and advice, and Prof. Francisco J. Sánchez-Sesma for many useful discussions. Daniel Bielak helped prepare the manuscript for publication. This research was supported by the U.S. National Science Foundation's Grand Challenge program, under grant CMS-9318163. The cognizant NSF program director is Dr. Clifford J. Astill. Computing services on the Pittsburgh Supercomputing Center's Cray T3D were provided under grant BCS-960001P. We are grateful for this support.

REFERENCES

- Adams, B., et al (1999), Report 99-3, Dept. of Civil Engrg., University of Canterbury, Christchurch, New Zealand.
Aki, K. (1977), in J.L. von Thun, ed., *Earthq. Engrg. And Soil Dyn.II: Recent Adv. In Ground-Motion Eval.*, pp. 103-155.
Bao, H. (1998), Ph.D. Thesis, Carnegie Mellon University., Pittsburgh, PA.
Bao, H. et al (1998), *Comput. Methods Appl. Mech. Engrg.*, Vol. 152, pp. 85-102.
Bard, P.Y. and M. Bouchon (1985), *Bull. Seism. Soc. Am.*, Vol. 75, pp. 519-541.
Bielak, J., J. Xu, and O. Ghattas (1999), *J. Geotech. Geoenv. Engrg.*, ASCE, Vol. 125, pp. 413-423.
Frankel, A. (1993) *Bull. Seism. Soc. Am.*, Vol. 83, pp. 1020-1041.
Graves, R.W. (1996), *Bull. Seism. Soc. Am.*, Vol. 86, pp. 1091-1106.
Graves, R.W. (1998) 2nd Int. Symp. on ESG, Special Volume on Simultaneous Simulations for Kobe, pp. 47-52, Japan.
Hartzell, S., et al (1996), *Bull. Seism. Soc. Am.*, Vol. 86, pp. S168-S192.
Herrera, I. and E. Rosenblueth (1965), *Third World Conf. Earthq. Engrg.*, Vol. 1, pp. 44-60, Rome, Italy.
Hisada, Y. (1995) *Bull. Seism. Soc. Am.*, Vol. 85, pp. 1080-1093.
Hisada, Y. and S. Yamamoto (1996), *Eleventh World Conf. Earthq. Engrg.*, Paper No. 2040, Acapulco, Mexico.
Hisada, Y. et al, 2nd Int. Symp. on ESG, Special Volume on Simultaneous Simulations for Kobe, pp. 59-66, Japan
Kanai, K.T., T. Tanaka, and S. Yoshizawa (1959), *Bull. Earthq. Res. Inst.*, University of Tokyo, Vol. 37, pp. 53-87.
Kawase (1966), *Seism. Res. Lett.*, Vol. 67, pp. 25-34.
Matsushima, S. and H. Kawase, 2nd Int. Symp. on ESG, Special Volume on Simultaneous Simulations for Kobe, pp. 59-66, Yokohama, Japan
NEHRP (1997), *NEHRP Recommended Provisions for the Development of Seismic Regulations for Buildings*, Building Seismic Safety Council, FEMA.
Olsen, K.B. and R.J. Archuleta (1996), *Bull. Seism. Soc. Am.*, Vol. 86, pp. 575-596.
Pitarka, A. and K. Irikura (1998), *Bull. Seism. Soc. Am.*, Vol. 88, pp. 428-440.
Reglamento (1993), *Reglamento de Construcciones para el DF*, Mexico.
Roesset, J. M. (1970), in R.J. Hansen, ed., *Seismic design for nuclear power plants*, pp. 183-244
Sánchez-Sesma, F.J. and F. Luzón (1995), *Bull. Seism. Soc. Am.*, Vol. 85, pp. 269-284.
Satoh, T., H. Kawase, and T. Sato (1995), *Bull. Seism. Soc. Am.*, Vol. 85, pp. 1821-1834.
Wald, D. (1995), *Seism. Res. Lett.*, Vol. 66, pp. 22-28.
Yegian, M.K., V.G. Ghahraman, and G. Gazetas (1994), *J. Geotech. Eng.*, ASCE, Vol. 120, pp. 349-365.